International Journal Of
Industrial Electronics Control and Optimization
Print ISSN: 3517-2645
Online ISSN: 3568-2645
Homepage: https://ieco.usb.ac.ir/

# An Optimal Self-Tuning Fuzzy Tilted Integral Derivative Controller for Load Frequency Control of Multi-Interconnected Power Plants

Morteza Janfaza[1] | Abbas-Ali Zamani[2]

Department of Electrical Engineering, Faculty of Engineering, University of Saravan, Saravan, Iran.[1]
Department of Electrical Engineering, National University of Skills (NUS), Tehran, Iran.[2]
Corresponding author's email: m.janfaza@saravan.ac.ir

**Article Info**

**Article type:**
Research Article

**Article history:**
Received: 02-June-2024
Received in revised form: 03-August-2024
Accepted: 06-August-2024
Published online: 21-Dec-2024

**Keywords**:
Load frequency control,
Multi-source power systems,
self-tuning fuzzy,
Renewable energy sources,
Tilted integral derivative.

**ABSTRACT**

A new framework for controlling load frequency in a complex, interconnected power system with multiple sources has been developed. This framework combines a fuzzy logic controller (FLC) and a tilted integral derivative (TID) controller, creating a self-tuning fuzzy tilted integral derivative (STFTID) controller. The purpose of this controller is to conduct and reduce load frequency perturbations during the operation of a multi-area interconnected multi-source power system. The STFTID controller is optimized using a particle swarm optimization algorithm to minimize the frequency fluctuations effectively. Investigations of the proposed STFTID controller were performed for power systems with generation units of a conventional system and renewable energy sources. In the design process of the STFTID controller, various nonlinearities, uncertainties, and fluctuations are considered to simulate practical challenges. These challenges include generation rate constraints, governor deadband, and communication time delays (as the sources of nonlinearity), as well as fluctuations caused by step load switching and the connection of renewable power plants to the system. The STFTID controller is compared with the proportional integral derivative (PID), titled integral derivative, and integral tilted-derivative (I-TD) controllers. Simulation results show that the developed STFTID controller significantly enhances the system frequency control under various applied conditions, including multi-step load perturbation, renewable power plant integration, communication time delays, and generation rate constraints.

## I. Introduction

The power system has the critical task of maintaining a balance between the supply of electricity and the demand for it. This delicate balance can be influenced by uncertainties on either the demand side or the supply side. Moreover, hybrid power systems are designed to address the integration between conventional and renewable energy sources (RESs) for power generation. The discrepancies that may arise between the generation of electricity and its consumption may be increased in such cases, especially when the weather and daylight cause severe switching oscillations in the system's response. By integrating multiple RESs, such as wind and solar energy, these systems can improve overall efficiency and achieve an optimal balance in electricity generation [1, 2]. However, the connection of such systems to the power grid may introduce perturbations to the output frequency and power.

Nowadays, the new challenges that hybrid power systems face are unpredictable because of the intrinsically volatile nature of the RESs and the variations in power demand. Therefore, integrating the RESs into the power grid system

decreases inertia, negatively affecting system stability in higher load frequency and power deviations. Conventional power-generating systems face such challenges, but they become more severe when RESs are added to the grid, impacting the reliability and safety of the power system [3, 4]. To maintain a steady grid frequency and manage the power distribution between various power system regions, it is crucial to have load frequency control (LFC) [5-8].

To control power systems, various control methods have been employed to address the LFC problem. These methods include robust control [9, 10], model predictive control [11, 12], fuzzy logic control [13, 14], and artificial intelligence control [15, 16]. Furthermore, PID controllers have attracted the attention of researchers due to their effectiveness and relatively simple implementation [17, 18]. However, determining the appropriate PID parameters can be challenging, especially when dealing with uncertain or nonlinear systems. This often requires trial-and-error techniques. To tackle this challenge, one can employ numerical optimization algorithms to calculate the best PID parameters [19-22]. Overcoming the fluctuations of real power and load angle of a synchronous generator in both transient and permanent conditions of the system and expanding the range of stable operation of the generator using a PID controller, is one of the important issues in power systems [19]. In [20], a PID controller is used to control the real output power and load angle of the synchronous generator, whose parameters are set using the genetic algorithm. The Harris Hawk optimization algorithm is used to optimally adjust the coefficients of the PID controller to control the load angle of a synchronous generator [21]. In [22], using an arithmetic optimization algorithm, PID controller coefficients are set with two approaches reducing the settling time and reducing the amount of overshoot of the step response to control the load angle of a three-phase synchronous generator.

Furthermore, there has been increased research focus on using fractional-order (FO) controllers in recent years. The reason behind such interest in FO controllers is their ability to expand the stability range and provide more flexibility in controller design [23, 24]. Specifically, the TID controller, which falls under the category of FO controllers, has been utilized to address LFC issues [25]. This controller effectively handles disturbances, meets the required specifications for the closed-loop system, and ensures a satisfactory level of robustness [25-27]. An optimal TID controller for the LFC problem is constructed in [28] by taking a cost function into account and applying a GA algorithm. For a two-area multi-source interlinked power system made up of thermal-hydro-gas generating units with nonlinearities, a cascade type of TID controller is suggested in [29]. In [30], an optimal TID controller is formed for the LFC problem of a multi-area networked reorganized power system. With the use of a hungry games search algorithm, the recommended TID controller settings are adjusted. However, a significant challenge in this research area remains unsolved: the controller parameters of the TID controller are considered fixed after optimization in the design phase and cannot be modified dynamically.

Several authors have recommended the utilization of the Fuzzy Logic Controller along with the conventional controllers to improve the performance of the LFC system [13, 14]. In a fuzzy control system, the input variables are usually represented by fuzzy sets. These sets consist of membership functions (MFs) that can be adjusted to obtain the desired efficiency of the system. Several algorithms have been proposed in the literature to modify the gains of the fuzzy controller, including the Whale Optimization Algorithm [31], the Ennoble Class Topper Algorithm [32], and the Particle Swarm Optimization (PSO) [13, 14]. Furthermore, for frequency stability in hybrid systems, a Fuzzy-PIDF controller has been presented based on the PSO algorithm and the Competition over Resources (COR) method [33]. Moreover, a fuzzy self-tuning PID controller has also been proposed for LFC that uses the Tribe-DE optimization method to handle parametric uncertainties and external disturbances. Previous fuzzy-based LFC structures have shown satisfactory system responsiveness. However, these controllers cannot be considered fully optimized because only the input and output scaling factors were optimized in these structures. Additionally, the limitations of the membership functions were solely determined based on the designer's expertise and may not be fully optimized [34].

This study introduces a new adaptive framework called the self-tuning fuzzy tilted integral derivative controller, dedicated to LFC of power systems. This controller addresses the issues with the FLC and TID controllers mentioned earlier. The STFTID parameters are adjusted using the PSO algorithm. Then, two-area interconnected power systems are considered to evaluate the performance of the proposed STFTID controller based on PSO: one system for conventional power generating systems and another for RESs. In the first two-area interconnected power system, each area consists of various traditional generation units (thermal, gas, and hydraulic power plants). In contrast, in the second one, renewable generation units (wind and solar power) are considered. The design of the proposed controller considers various nonlinearities in the system, including generation rate constraints, governor deadband, and communication time delays. It also addresses uncertainties in the fluctuations in load and RESs.

To validate the effectiveness of the STFTID controller, its performance is investigated by comparing it with other control techniques discussed in the literature, including the PID controller, TID controller, and I-TD controller. The I-TD controller is an improved version of the TID controller proposed for the LFC of a power system in [35-37]. The paper's contributions are summarized as follows.

- A load frequency control framework based on a self-tuning fuzzy tilted integral derivative controller is proposed.
- The proposed STFTID combines a fuzzy logic controller and a tilted integral derivative controller.
- A hybrid power system including various conventional generation units (thermal, gas, and hydraulic power plants), and renewable generation units (wind and solar power) is considered for evaluating the proposed STFTID.
- The performance assessments of the proposed STFTID controller are done taking into account various nonlinearities in the system, including generation rate constraints, governor deadband, and communication time delays.
- The performance of the proposed STFTID controller is compared with traditional PID, TID, and I-TD controllers.
- The improvement of performance indicators of the proposed STFTID controller was evaluated and shown during four different scenarios.

The organization of the remains of the paper is as follows: Section 2 introduces the description of the hybrid power system models investigated in this study. Section 3 describes the PSO algorithm used for optimization. Section 4 focuses on the structure of the proposed STFTID controller. In Section 5, the parameters of the system being studied are presented, as well as the definition of four different scenarios. Then, the proposed control method is numerically analyzed, and the improved performance of the proposed STFTID structure is studied and discussed for these scenarios. Finally, the conclusion is presented in the last section.

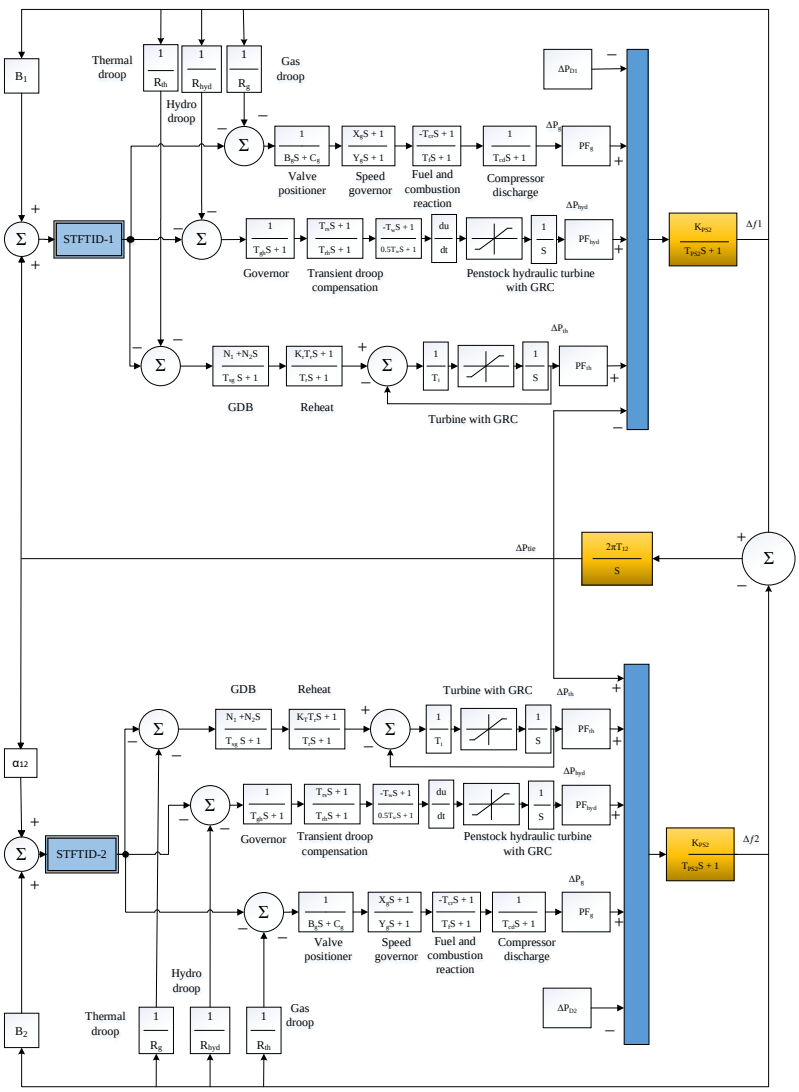


Fig. 1. The interconnected dynamic model for a two-area multi-source power system, including gas, hydro, and reheat thermal power plants.

## II. Dynamic Modeling of the Studied Power System

Firstly, we have examined a two-area diverse-unit power system [35-37]. Fig.1 shows the MATLAB SIMULINK modeling structure used for this purpose. The assumption for this structure is presented here.

There are dedicated building blocks for different power plants in these areas, including i) gas, ii) hydro, and iii) reheat thermal power plants. The gas power plant contains transfer functions for the valve positioner, speed governor, fuel and combustion reaction, and compressor discharge. The transfer functions are shown in the building blocks of Fig. 1. The hydro power plant comprises its governor, transient droop compensator, and a penstock hydraulic turbine with a generation rate constraint (GRC). The reheat thermal power plant includes a governor deadband (GDB), and its transfer function provides the input for a turbine with a nonlinear steam turbine and a GRC.

GDB and GRC limit the capability of the power system to reject disturbances immediately. Therefore, reliable, realistic, and precise results depend on the considered physical constraints and multi-source power generations in each control unit/area. To study such effects, we define the GDB as a function of the sustained speed change magnitude resulting from mechanical frictions, valve overlaps in hydraulic relays, and backlash. It should be noted that the position of the valve in the thermal turbine is considered fixed. GDB prevents immediate reaction of the governor until the input reaches a specific value. This increases the fluctuations, and the stability of the power system reduces accordingly. Such an effect leads to sinusoidal oscillations with a fundamental frequency of 0.5 Hz. GDB equation nonlinearity may be decreased by variations in the speed/speed rate. The linear model for a GDB with 0.5% backlash can be written as Eq. 1.

$$GDB = \frac{N_1 + N_2 S}{T_{sg} S + 1} \tag{1}$$

This model is solved for $N_1$= 0.8 and $N_2$= -0.2/π for the reheat thermal power plant.

GRC allows for the maximum variations of the practical generation rate for both the hydro and thermal units. For the rising and falling rates of the hydro unit, generation variations of 270% and 360% are assumed, respectively, while a GRC of 10% is considered for the reheat thermal units [35-37].

The effects of renewable energy penetrations are modeled by dynamic blocks of a two-area power system for wind and solar energies, as shown in Fig. 2. These units are modeled based on the assumptions and considerations of Sections 2.1 and 2.2, respectively.

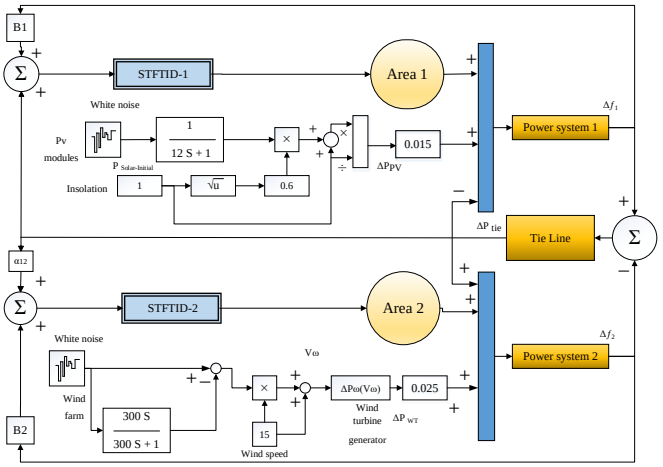


Fig. 2. The interconnected dynamic model for a two-area double-source power system, including PV and wind power plants.

### A. PV System Model

The PV system is constantly affected by diverse environmental factors. Such factors, including seasonal changes in sun irradiation, variations in irradiation time during the 24-hour day, and weather conditions, should be considered. Additionally, the irregular output power of the PV systems generates significant frequency deviations, posing a threat to the stability of the system. Thus, careful consideration should be given to both the uniform and non-uniform deviations in insolation when estimating the output power of PV systems. To this end, the oscillated output power of this system is simulated using white noise. These variations are then added to the output power of the PV system [35-37]:

$$\Delta P_{Solar} = 0.6\sqrt{P_{Solar}} \tag{2}$$

### B. Wind Generation Unit Model

The behavior of the wind is random as well. To account for this randomness, another white noise block is applied to multiply the wind speed. Consequently, the computed output power from the wind generation unit ($P_W$) is determined by equation (3) [35-37], where the density of air, the area swept by the rotor, and the wind-rated speed are represented as $\rho$, $A_T$, and $V_W$, respectively.

$$P_W = \frac{1}{2}\rho A_T V_W^3 C_P(\lambda, \beta) \tag{3}$$

Moreover, the parameter of the rotor blades is given by $C_P$ as in (4);

$$C_P(\lambda, \beta) = C_1 \times \left(\frac{C_2}{\lambda_I} - C_3\beta - C_4\beta^2 - C_5\right) \times e^{\frac{C_6}{\lambda_I}} + C_7\lambda_T \tag{4}$$

Here, coefficients $C_1$ to $C_7$ represent the wind turbine parameters (see Table 1), and the pitch angle is $\beta$. Furthermore, $\lambda_T$ and $\lambda_I$ are the optimum tip-speed ratio (TSR) and the intermittent TSR, which can be calculated from (5) and (6):

$$\lambda_T = \lambda_T^{OP} = \frac{\omega_T \times r_T}{V_W} \tag{5}$$

$$\frac{1}{\lambda_I} = \frac{1}{\lambda_T + 0.08\beta} - \frac{0.035}{\beta^3 + 1} \tag{6}$$

In (5), $\omega_T$ and $r_T$ are the rotational speed and the radius of the rotor, respectively. Therefore, $P_W$ can be calculated as 750 kW for the coefficients of Table 1.

TABLE 1 THE PARAMETERS OF THE WIND GENERATION UNIT [35-37]

| Coefficient | Value | Coefficient | Value |
|---|---|---|---|
| $C_1$ | $-0.6175$ | $\rho$ | 1.225 Kg · m$^3$ |
| $C_2$ | 116 | $A_T$ | 1684 m$^2$ |
| $C_3$ | 0.4 | $V_W$ | 15 m/s |
| $C_4$ | 0 | $r_T$ | 22.9 m |
| $C_5$ | 5 | $\lambda_T$ | 22.5rpm |
| $C_6$ | 21 | $P_W$ | 750KW |
| $C_7$ | 0.1405 | $P_W$ | 750KW |

The photovoltaic (PV) system and wind power plants of Fig. 2 are connected to areas 1 and 2, with power rates of 50 MW and 70 MW, respectively. The obtained output power deviations, calculated with the model for the PV power plant and the wind turbine, are shown in Fig. 3.

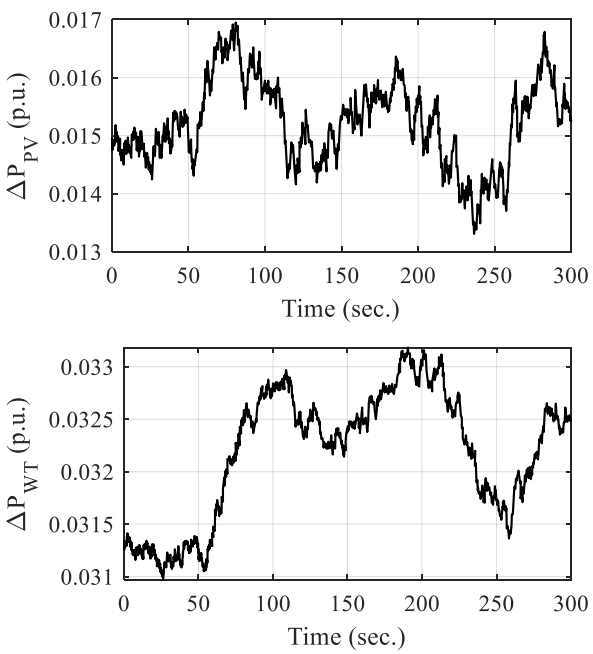


Fig. 3. The RESs output power deviations are calculated from the model shown in Fig. 2.

## III. Particle Swarm Optimization Algorithm

PSO is an optimization technique in which a simplified social model simulates populations called swarms. Each population is composed of particles (similar to a bird's swarm), in which the particles fly through the problem space and look for the optimal position, just as a bird swarm searches for food. This evolutionary technique solves multiple conditions simultaneously and collaborates on the solutions to yield the final results. Each particle corrects its position based solely on the knowledge from its own experience and that of its neighbors. The initial population is random, while the algorithm updates the particles and populations in generations.

For an *N*-dimensional search space, particle *i* has N-dimensional position and velocity vectors, namely $x_i$ = ($x_{i1}$, $x_{i2}$, ..., $x_{iN}$) and $v_i$ = ($v$ $v_{i1}$, $v_{i2}$, ..., $v_{iN}$), respectively. The objectives of the optimization problem monitor the fitness of particles, and the best position previously visited by particle i is considered as its best experience and indexed as $Pi$ = ($p_{i1}$, $p_{i2}$, ..., $p_{iN}$), while the best position of the whole population is considered as the best global position, indexed as $G$ = ($g$ $g_1$, $g_2$, ..., $g_N$).

Having data for each search step, i.e., $x_i$, $v_i$, $P_i$, and $G$, the new positions of each particle change according to the x and v vectors based on Eq. 7. In Eq. 7, w represents the inertia weight which controls the impact of the v vector from previous steps, $r_j$, and $c_j$ are random variables (in the range of [0, 1]) and positive acceleration constants, respectively.

$$v_i(k+1) = w^2 v_i(k) + c_1 \cdot r_1 \cdot (P_i(k) - x_i(k)) + c_2 \cdot r_2 \cdot (G(k) - x_i(k)) \tag{7}$$

$$x_i(k+1) = x_i(k) + v_i(k) \tag{8}$$

The velocity vector is limited in the range of [-$v_{max}$, and $v_{max}$], so that the particle's roaming outside the search space can be controlled, and excessive roaming is prevented.

## IV. Proposed Self-Tuning Fuzzy Tilted Integral Derivative Controller

The most crucial aspect of operating an interconnected power system is ensuring frequency stability. Fluctuations in such systems arise from an imbalance between production and demand. In real-world scenarios, electrical loads within a power system are constantly changing. Consequently, the production rate must be carefully managed to maintain a sustained balance between production and demand. To achieve such a balance, the power system should be able to restructure the integration between the conventional power units and the RESs. In order to study the behavior of the operation and control of a power system, uncertainties should be considered during standard operational intervals. Various technical problems can be used to reduce system fluctuations and maintain a balanced production and demand cycle [1, 2]. The STFTID controller proposed in this section is a self-tuning fuzzy-based structure that utilizes a TID controller, as shown in Fig. 4.

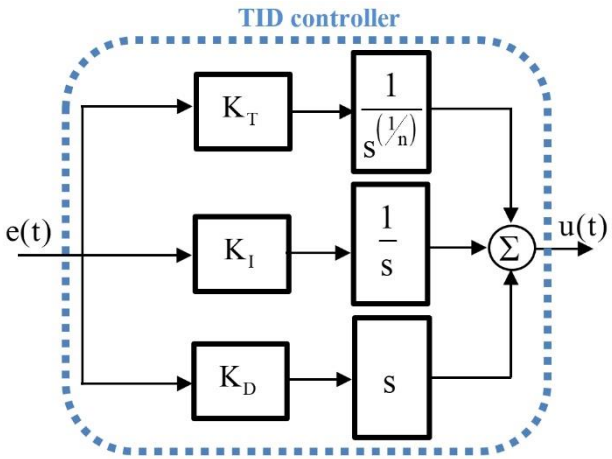


Fig. 4. The tilted integral derivative controller scheme.

The TID controller offers enhanced performance and control, with increased sensitivity to system parameter variations and improved disturbance rejection. System tuning is also made more accessible [27, 35, 38]. As is obvious from Fig. 4, the structure of the TID controller is similar to a PID, in which the proportional component is replaced by a titled integral derivative with a transfer function of $1/s^{1/n}$. In other words, for a PID controller, the transfer function is generally shown as (9), while it is modified as (10) for a TID.

$$PID = K_P + \frac{K_I}{S} + K_D S \tag{9}$$

$$TID = \frac{K_T}{S^{(1/n)}} + \frac{K_I}{S} + K_D S \tag{10}$$

With $K_P$, $K_T$, $K_I$, and $K_D$ as the proportion, proportional tilt gain, integral, and differential coefficients, the transfer functions govern the controller systems. Moreover, the tilt fractional component is shown by n in (10) which may be tuned in the valid range of [1 10]. The modified system performance is a result of considering the tilt fractional component *n*, allowing the improved system performance to face disturbances and uncertainties. Therefore, the overall tuning process can be simplified. Additionally, a self-adjusting control structure is crucial in new power systems with diverse sources of uncertainty. Thus, a self-tuning fuzzy tilted-integral-derivative controller is proposed to regulate the load frequency, utilizing the advantageous TID controllers illustrated in Fig. 5. This STFTID structure is employed in a system comprising *i* regions.

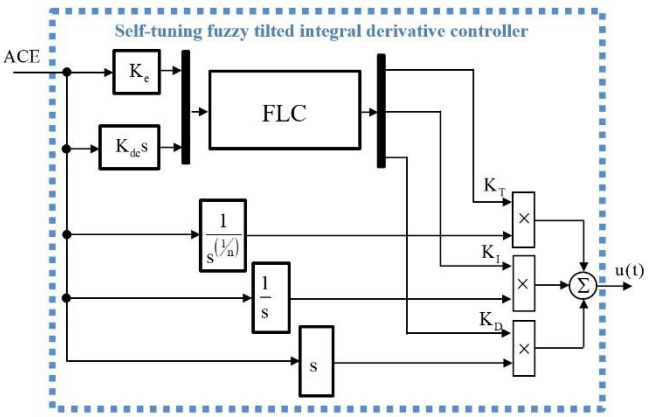


Fig. 5. The proposed optimal STFTID control structure.

The FLC block in the STFTID control structure of Fig. 5 is a Mamdani type, including two inputs and three outputs, which sets the values of the TID controller coefficients for areas in a self-tuning manner. Coefficients $K_T$, $K_I$, and $K_D$, get values based on the rules summarized in Table 2. In this table, NB, N, Z, and P show negative, zero, and positive values, respectively. In contrast, S, M, and B abbreviate small, middle, and significant values, and V is the acronym for the word "very".

TABLE 2 RULES FOR THE FUZZY CONTROLLER USED IN THE PROPOSED CONTROLLER.

| $K_T, K_I, K_D$ | | $\frac{dACE}{dt}$ | | | | | | |
|---|---|---|---|---|---|---|---|---|
| | | NB | NM | NS | Z | PS | PM | PB |
| $ACE$ | NB | VB/VS/M | VB/VS/SM | B/S/S | B/S/VS | BM/SM/S | BM/M/SM | M/M/M |
| | NM | VB/VS/M | B/S/SM | B/S/S | BM/S/VS | BM/M/S | M/M/SM | SM/M/M |
| | NS | B/S/M | B/S/SM | BM/SM/S | BM/M/VS | M/M/S | SM/M/SM | SM/BM/M |
| | Z | B/S/BM | BM/SM/M | BM/M/SM | M/M/S | SM/M/SM | SM/BM/M | S/B/BM |
| | PS | BM/SM/B | BM/M/BM | M/M/M | SM/M/SM | SM/BM/M | S/B/BM | S/B/B |
| | PM | BM/M/VB | M/M/B | SM/M/BM | S/BM/M | S/B/BM | S/B/B | VS/VB/VB |
| | PB | M/M/VB | SM/M/B | SM/BM/B | S/B/BM | S/B/B | VS/VB/B | VS/VB/VB |

The self-tuning manner of the STFTID controller of Fig. 4, working based on the rules applied by Table 2, updates the values of $K_T$, $K_I$, and $K_D$ to feed the TID controller structure. This is repeated for each time step, while the value of parameter n and two scaling factors $K_e$ and $K_{de}$ are updated based on implementing the optimization process in these steps. The style of input membership functions for the fuzzy block is exhibited in Fig. 6.

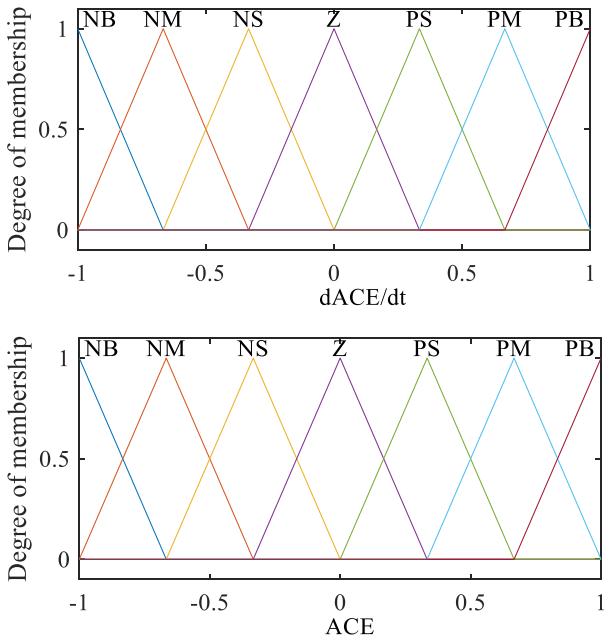


Fig. 6. The input MFs for the STFTID controller.

The $K_T$, $K_I$, and $K_D$ represent the outputs from the fuzzy block. These MFs of the outputs are illustrated in Fig. 7, wherein $B_T$, $B_I$, and $B_D$ are considered for the parameters of the upper bands. During the design process, a PSO algorithm can specify these parameters. When the values of $B_T$, $B_I$, and $B_D$ are determined, the following equations are employed to calculate the magnitude of the output membership functions' centers.

$$\begin{aligned} a_1^i &= \frac{1}{6}B_i \\ a_2^i &= \frac{2}{6}B_i \\ a_3^i &= \frac{3}{6}B_i \\ a_4^i &= \frac{4}{6}B_i \\ a_5^i &= \frac{5}{6}B_i \end{aligned} \tag{11}$$

Here, index $i$ is set as $T$, $I$, and $D$ to satisfy all the necessary parameters. For the optimal design process in our proposed controller, a design vector $X_D$ is used as shown in (12):

$$X_D = [B_T, B_I, B_D, K_e, K_{de}, n]. \tag{12}$$

To complete the optimization procedure, a cost function was also used in the STFTID controller based on (13).

$$G_c(X_D) = \int_{t=0}^{t=T_{sim}} t.((\Delta f_1)^2 + (\Delta f_2)^2 + (\Delta p_{tie})^2)dt \tag{13}$$

Finally, the design intervals for the parameters are considered based on (14).

$$\begin{aligned} &0 < B_T \le 10 \\ &0 < B_I \le 10 \\ &0 < B_D \le 10 \\ &0 < K_e \le 1 \\ &0 < K_{de} \le 1 \\ &1 \le n \le 10 \end{aligned} \tag{14}$$

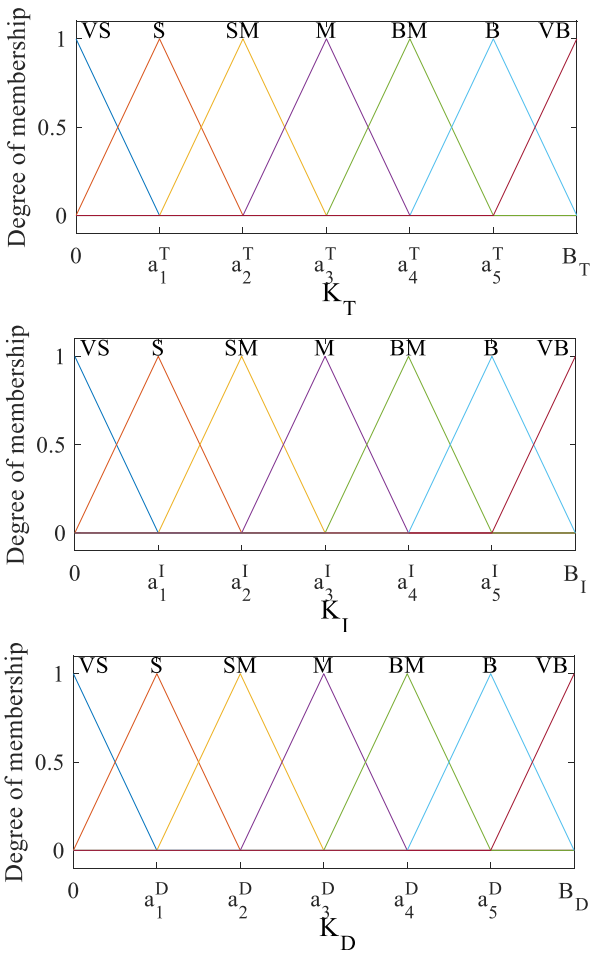


Fig. 7. The considered output membership functions for the STFTID controller.

## V. Performance Validation and Simulation Results

To validate the performance of the proposed controller, four different scenarios were investigated and the results from the proposed STFTID controller were compared to [36-38]. The parameters of the hybrid power system are as follows: The governor speed regulation parameters of the gas, hydro, and thermal units are $R_g$=$R_{hyd}$=$R_{th}$=2.4. The first and second Fourier coefficients in the GDB transfer function are $N_1$=0.8 and $N_2$=-0.2/π, respectively. The time constants of the transient droop, Governor of the steam turbine, and steam turbine are $Trh$=28.749, $Tsg$=0.06, and $Tt$=0.3, respectively. The starting time of water in the hydro turbine, the steam turbine reheats constant, and the steam turbine reheat time constant are $T_w$=1.1, $K_r$=0.3, and $T_r$=10.2, respectively.

The first and second power system time constants are $T_{ps1}$=$T_{ps2}$=11.49. The first and second power system gains are $K_{ps1}$=$K_{ps2}$=68.965. The synchronizing coefficient is $T_{12}$=0.0433. The participation factors of gas, hydro, thermal, PV system, and wind generation units are $PF_g$=0.2873, $PF_{hyd}$=0.138, $PF_{Th}$=0.5747, $PF_{pv}$=0.015, and $P_{FWT}$=0.025, respectively. The lead and lag time constant of gas turbine governor are $X_g$=0.6, and $Y_g$=1.1. The time constant of the value positioner, Hydro turbine governor, and Compressor discharge volume are $B_g$=0.049, $T_{gh}$=0.2, and $T_{cd}$=0.2, respectively. The valve positioner, fuel time constant, and combustion reaction time delay of the gas turbine are $C_g$=1, $T_f$=0.239, and $T_{cr}$=0.01, respectively. The hydro turbine speed governor reset time and frequency bias coefficients are $T_{rs}$=4.9 and $B_1$=$B_2$=0.4312.

### *A. First Scenario*

For the first scenario, we compared our proposed STFTID controller with the PID, TID, and I-TD controllers in [35], with a 1% step load only in the first area of the two-area power system shown in Fig. 1. The comparison was based on the parameters listed in Table 3 for the STFTID controller parameters.

TABLE 3 PARAMETERS OF THE PROPOSED STFTID CONTROLLER FOR THE FIRST SCENARIO

| | $B_T$ | $B_I$ | $B_D$ | $K_e$ | $K_{de}$ | n |
|---|---|---|---|---|---|---|
| Area-1 | 8.5316 | 9.0135 | 6.1037 | 0.3912 | 0.4692 | 2.1976 |
| Area-2 | 5.9136 | 6.8601 | 4.0671 | 0.4168 | 0.5318 | 2.3671 |

The results of Fig. 8 confirm the convergence between the output of all considered controllers. As can be seen from the results of this figure, the characteristics of the TID and I-TD controllers are better than those of the PID. The STFTID performance is the best in terms of the maximum overshoot and undershoot (MO and MU), as well as the settling time (ST), rise time (RT), peak time (PT), and the index of the integral time square error (ITSE). To quantify these factors to evaluate of the dynamic system performance, they are summarized in Table 4.

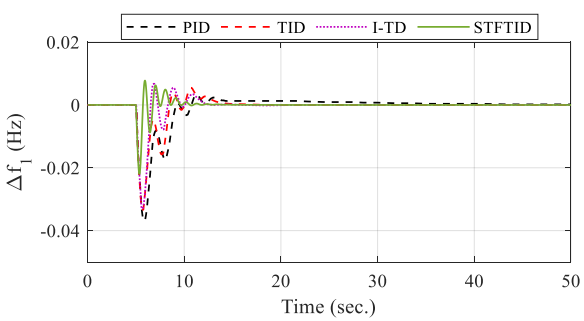


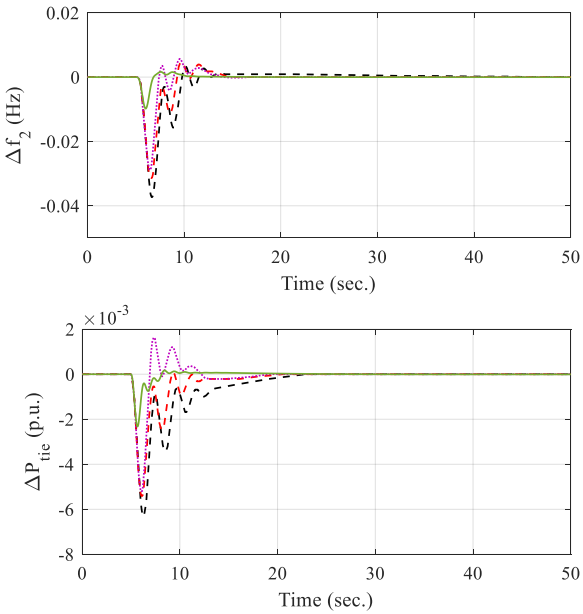


Fig. 8. The time history of the studied controllers for the first scenario.

TABLE 4 THE DYNAMIC SYSTEM PERFORMANCE INDICES FOR THE FIRST SCENARIO.

| | | PID | TID | I-TD | STFTID |
|---|---|---|---|---|---|
| $\Delta f_1$ | ST | 25 | 15 | 11 | 10 |
| | MO | 0.004 | 0.005 | 0.006 | 0.006 |
| | MU | -0.04 | -0.034 | -0.033 | -0.021 |
| | RT | 1.01 | 0.92 | 0.88 | 0.31 |
| | PT | 6.21 | 5.82 | 5.76 | 5.41 |
| | | PID | TID | I-TD | STFTID |
| $\Delta f_2$ | ST | 30 | 16 | 13 | 7.5 |
| | MO | 0.001 | 0.005 | 0.0051 | 0.001 |
| | MU | -0.038 | -0.031 | -0.029 | -0.010 |
| | RT | 1.28 | 0.94 | 0.90 | 0.26 |
| | PT | 6.76 | 6.11 | 5.98 | 5.54 |
| | | PID | TID | I-TD | STFTID |
| $\Delta P_{tie}$ | ST | 20 | 25 | 25 | 8 |
| | MO | 0 | 0 | 0.002 | 0.0001 |
| | MU | -0.006 | -0.005 | -0.005 | -0.002 |
| | RT | 1.22 | 0.91 | 0.84 | 0.26 |
| | PT | 6.49 | 6.02 | 5.87 | 5.32 |
| | | PID | TID | I-TD | STFTID |
| ITSE | | 0.0056 | 0.0035 | 0.0022 | 0.0007 |

### *B. Second Scenario*

To further evaluate the performance of the proposed STFTID controller, in the second scenario, we applied a multi-step load perturbation (MSLP) to area 1 of the two-area power system shown in Fig. 1 to simulate a more realistic situation. This MSLP, shown in Fig. 9, can represent a series of forced shutdowns occurring for the power-generating units, and unexpected loading switches. The results of the system's response are shown in Fig. 10 for different controllers, namely TID, I-TD, and STFTID, for this scenario.

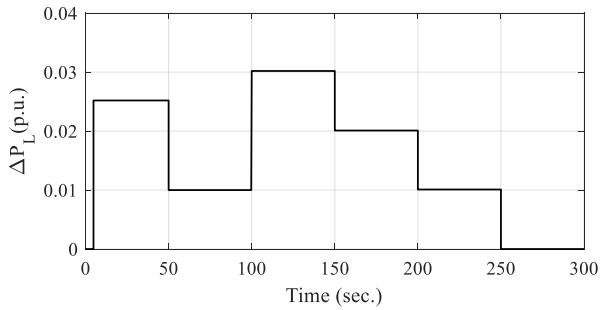


Fig. 9. The step load pattern for the second scenario.

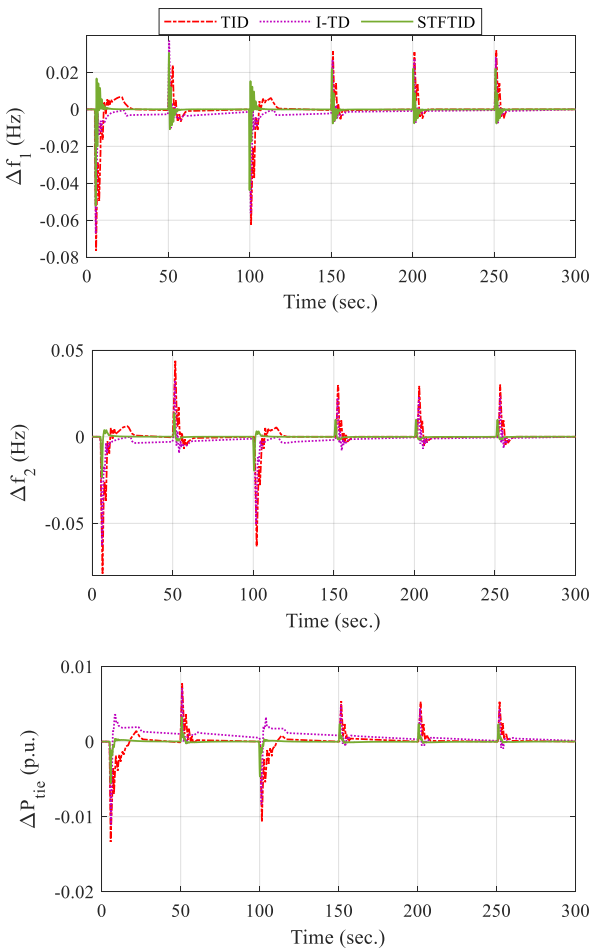


Fig. 10. The time history of the studied controllers for the second scenario.

The optimized parameters for the proposed STFTID are summarized in Table 5, whereas the dynamic system performance under this situation can be seen in Table 6. As is evident from Fig. 10 and Table 6, the best ST, MO, MU, RT, and PT are the results of the proposed STFTID, for all the loading variations of the applied MSLP. Therefore, this STFTID controller can be a practical, high-performance solution for the LFC problems, giving the best damping performance for the forced MSLP.

TABLE 5 PARAMETERS OF THE PROPOSED STFTID CONTROLLER FOR THE SECOND SCENARIO.

| | $B_T$ | $B_I$ | $B_D$ | $K_e$ | $K_{de}$ | n |
|---|---|---|---|---|---|---|
| Area-1 | 7.6319 | 8.9137 | 5.6186 | 0.4961 | 0.4169 | 2.9135 |
| Area-2 | 5.3619 | 6.0371 | 3.9135 | 0.3916 | 0.4692 | 2.6912 |

TABLE 6 THE SYSTEM DYNAMIC PERFORMANCE INDICES FOR THE SECOND SCENARIO.

| | | TID | I-TD | TFTID |
|---|---|---|---|---|
| $\Delta f_1$ | ST | 20 | 200 | 10 |
| | MO | 0.05 | 0.03 | 0.03 |
| | MU | -0.08 | -0.07 | -0.04 |
| | RT | 1.06 | 1.26 | 0.86 |
| | PT | 5.56 | 5.87 | 5.21 |
| | | TID | I-TD | STFTID |
| $\Delta f_2$ | ST | 20 | 200 | 9 |
| | MO | 0.05 | 0.03 | 0.010 |
| | MU | -0.08 | -0.06 | -0.021 |
| | RT | 0.97 | 1.12 | 0.79 |
| | PT | 5.31 | 5.58 | 5.14 |
| | | TID | I-TD | STFTID |
| $\Delta P_{tie}$ | ST | 30 | 200 | 10 |
| | MO | 0.008 | 0.007 | 0.001 |
| | MU | − 0.014 | − 0.01 | -0.005 |
| | RT | 0.92 | 1.10 | 0.75 |
| | PT | 5.23 | 5.47 | 5.11 |
| | | TID | I-TD | STFTID |
| ITSE | | 35 | 25 | 3.11 |

### *C. Third Scenario*

The third scenario compares the performance of three controllers, i.e. TID, I-TD, and STFTID, under load disturbances with various applied patterns, as shown in Fig. 11. This scenario evaluates the performance of the proposed STFTID for RES fluctuations in the interconnected dynamic model shown in Fig. 2. To this end, three controllers under investigation are examined for solar energy and wind penetrations, wherein the PV system and the wind power plants are connected to area 1 and 2, respectively, with rated powers of 50 and 70 MW. The parameters for the STFID controller are presented in Table 7 for this scenario, and the maximum iteration and search number agents are set to 50 and 10.

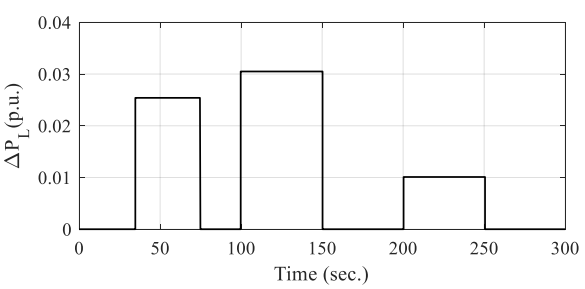


Fig. 11. The step load pattern for the third scenario.

TABLE 7 PARAMETERS OF THE PROPOSED STFTID CONTROLLER FOR THE THIRD SCENARIO.

| | $B_T$ | $B_I$ | $B_D$ | $K_e$ | $K_{de}$ | n |
|---|---|---|---|---|---|---|
| Area-1 | 4.3671 | 1.6138 | 2.9376 | 0.3371 | 0.4923 | 5.9637 |
| Area-2 | 3.8613 | 1.3812 | 3.3682 | 0.4631 | 0.5037 | 2.6381 |

This time, the simulations, including controllers under series load disturbance in area 1, as shown in Fig. 11, are performed for the wind power plant and the PV system connected after 100 and 250 s, respectively. It should be noted that this figure represents the frequency deviations for the two-area model and the variations of the tie-line power under the second scenario. One can easily conclude from the results of Fig. 12 (summarized in Table 8) that severe oscillations occur during the multistep load and RES connection time intervals for the frequencies and tie-line power. However, the proposed controller performance is superior to the TID and I-TD controllers and can reduce the ST in $\Delta f_2$ and $\Delta P_{tie}$. The TID performance is better for decreasing the ST for $\Delta f_1$. In all other evaluated parameters, i.e., MO, MU, and ITSE, the STFTID performance is superior to the TID and I-TD. In addition to this, the STFTID controller has better convergence compared to the other two controllers under investigation.

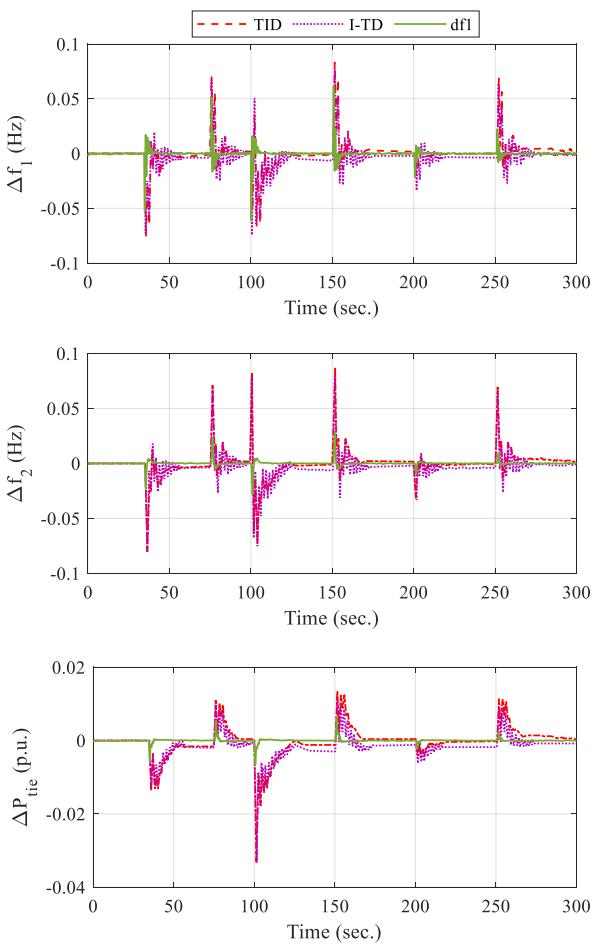


Fig. 12. The time history of the studied controllers for the third scenario.

TABLE 8 THE SYSTEM DYNAMIC PERFORMANCE INDICES FOR THE THIRD SCENARIO.

| | | TID | I-TD | STFTID |
|---|---|---|---|---|
| $\Delta f_1$ | ST | 120 | 150 | 150 |
| | MO | 0.07 | 0.06 | 0.05 |
| | MU | -0.07 | -0.06 | -0.05 |
| | RT | 1.11 | 1.25 | 0.93 |
| | PT | 101.95 | 102.86 | 101.02 |
| | | TID | I-TD | STFTID |
| $\Delta f_2$ | ST | 120 | 150 | 101 |
| | MO | 0.07 | 0.06 | 0.021 |
| | MU | -0.07 | -0.06 | -0.026 |
| | RT | 1.09 | 1.23 | 0.91 |
| | PT | 101.86 | 102.68 | 101.01 |
| | | TID | I-TD | STFTID |
| $\Delta P_{tie}$ | ST | 120 | 150 | 102 |
| | MO | 0.012 | 0.01 | 0.005 |
| | MU | -0.035 | -0.035 | -0.005 |
| | RT | 1.03 | 1.18 | 0.88 |
| | PT | 101.24 | 102.14 | 101.01 |
| | | TID | I-TD | STFTID |
| ITSE | | 28.12 | 23.45 | 12.55 |

### *D. Fourth Scenario*

In our last scenario, a 0.1 s communication time delay (CTD) was introduced to the controller's output. Additionally, load disturbances of 0.01 and 0.05 p.u. were considered for areas 1 and 2, respectively. In this scenario, the PV system and wind turbines were connected after 80 and 220 seconds, respectively, and the load disturbances were applied to areas 1 and 2 after 10 and 150 seconds. Based on the parameters in Table 9, the STFTID was configured, and its results are shown in Fig. 13 for TID, I-TD, and STFTID controllers.

TABLE 9 PARAMETERS OF THE PROPOSED STFTID CONTROLLER FOR THE FOURTH SCENARIO.

| | $B_T$ | $B_I$ | $B_D$ | $K_e$ | $K_{de}$ | n |
|---|---|---|---|---|---|---|
| Area-1 | 2.1394 | 2.1835 | 3.9613 | 0.3687 | 0.5316 | 1.6631 |
| Area-2 | 1.9385 | 1.8624 | 4.0136 | 0.4531 | 0.3286 | 1.8671 |

The perturbations in the output of the controller lead to oscillations of the system, as is evident in the frequency deviations of the two-area system, and the tie-line power response. Once again, the response of the proposed STFTID controller remains more stable, with significantly lower MO and MU values (see Table 10). However, the ST is also lower for the proposed controller than the TID and I-TD controllers.

From Fig. 13, it can be seen that more severe oscillations contribute to the system response at 150 and 220 s, while the step load disturbance in area 2 and the PV system connection occur. In both cases, the STFTID controller is more effective in dampening the oscillations. However, the TID shows worse performance.

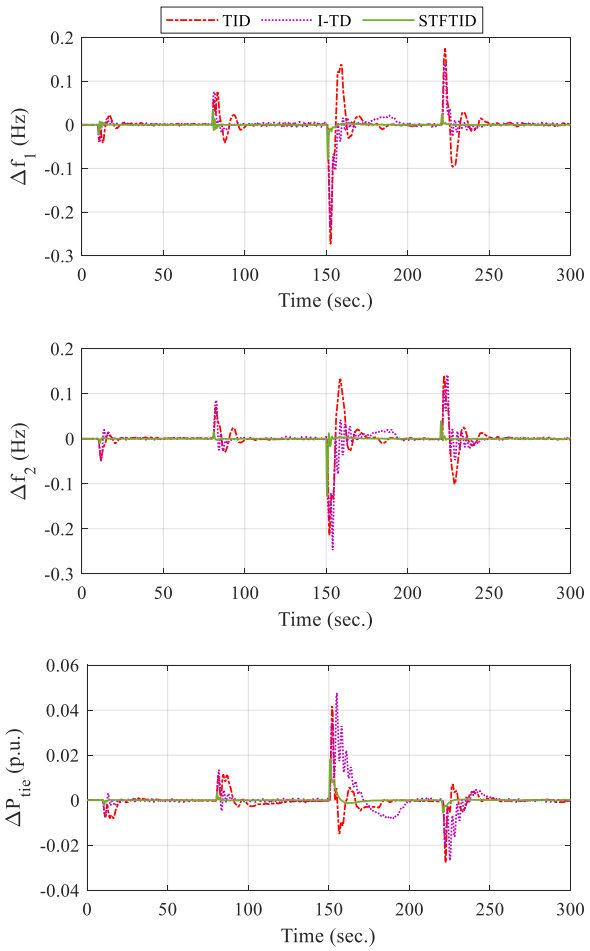


Fig. 13. The time history of the studied controllers for the fourth scenario.

TABLE 10 THE SYSTEM DYNAMIC PERFORMANCE INDICES FOR THE FOURTH SCENARIO.

| | | TID | I-TD | STFTID |
|---|---|---|---|---|
| $\Delta f_1$ | ST | 250 | 250 | 232 |
| | MO | 0.15 | 0.13 | 0.05 |
| | MU | -0.29 | -0.25 | -0.07 |
| | RT | 1.23 | 1.34 | 1.11 |
| | PT | 152.92 | 152.98 | 151.09 |
| | | TID | I-TD | STFTID |
| $\Delta f_2$ | ST | 250 | 250 | 223 |
| | MO | 0.1 | 0.1 | 0.05 |
| | MU | -0.25 | -0.2 | -0.11 |
| | RT | 1.21 | 1.26 | 1.09 |
| | PT | 152.65 | 152.71 | 151.05 |
| | | TID | I-TD | STFTID |
| $\Delta P_{tie}$ | ST | 250 | 250 | 223 |
| | MO | 0.05 | 0.04 | 0.017 |
| | MU | -0.02 | -0.02 | -0.005 |
| | RT | 1.18 | 1.20 | 1.02 |
| | PT | 152.13 | 152.16 | 150.98 |
| | | TID | I-TD | STFTID |
| ITSE | | 53.1 | 39.2 | 12.64 |

## VI. Results and Discussion

The preceding part presents the results of four scenarios in which the performance of the proposed STFTID controller is compared with that of the PID, TID, and I-TD controllers [35-37]. This allows for an evaluation of the controller's performance. In conclusion, the suggested STFTID controller can reduce the ST, MO, MU, RT, PT, and ITSE in every scenario.

In the first scenario, for example, the STFTID controller reduced the ST index for $\Delta f_1$ to 60%, 33.3%, and 9.1%, respectively, compared to the PID, TID, and I-TD controllers. These reductions for the MU index are 47.5%, 38.2%, and 36.4%, in that order. In comparison to the PID, TID, and I-TD controllers, the RT index for $\Delta f_2$ was reduced by the STFTID controller to 79.7%, 72.3%, and 71.1%, respectively. The PT index for $\Delta P_{tie}$ fell to 18%, 11.6%, and 9.4%, while the ITSE index also decreased to 87.5%, 80%, and 68.2%, respectively.

The ST index for $\Delta f_1$ dropped to 50% and 95% compared to the TID and I-TD controllers for the second scenario, which involves imposing an MSLP onto area 1 of a two-area power system. The MU index for $\Delta f_2$ has been reduced by 73.8% and 65%, respectively. The STFTID controller decreased the RT index for $\Delta P_{tie}$ to 18.5% and 31.8%, respectively, in contrast to the TID and I-TD controllers. In addition to the ITSE index, which dropped to 91.1% and 87.5%, respectively.

The third scenario results in a reduction in the MO index for $\Delta f_1$ to 28.6% and 16.7%, respectively, when renewable power plants are taken into account. Compared to the TID and I-TD controllers, the STFTID controller reduced the MU index for $\Delta f_2$ to 62.9% and 56.7%, respectively. Apart from the ST index for $\Delta P_{tie}$, which decreased to 15% and 32%, and the RT index fell to 14.6% and 25.4%, respectively. Also, the ITSE index fell to 55.3% and 46.5%, respectively.

In the fourth scenario, in addition to connecting the PV and wind power plants at different time steps, two-step load disturbances and a communication time delay were enforced. With a 66.7% and 61.5% drop in the MO index for $\Delta f_1$ compared to the TID and I-TD controllers, respectively, this scenario further demonstrates the superior performance of the STFTID controller. Apart from the MU index for $\Delta f_2$, which fell to 56% and 45%, respectively, there was a decrease in the ST index to 10.8% and 10.7%, a reduction in the RT index to 9.9% and 13.5%, respectively. Also, a significant decrease in the ITSE index to 76.2% and 67.8% was achieved, respectively. The findings collected from all scenarios show that the STFTID controller performs better than the PID, TID, and I-TD controllers in [35-37], despite having a more complex structure than the latter three kinds of controllers.

## VII. Conclusions

A control structure is presented in this paper, a self-tuning fuzzy tilted integral derivative control structure, to control the load frequency response of a hybrid power system.

The hybrid power system contains different power plants, including conventional (gas, hydro, and thermal plants) and renewable (PV and wind turbine). Nonlinear factors such as generation rates, governor deadband, and communication time delays are considered for the system. To evaluate the performance of the proposed STFTID control system, we present the results of four scenarios in which the results of STFTID are compared with those achieved by PID, TID, and I-TD controllers, confirming the performance of the proposed system. In summary, this system can mitigate the settling time, rise time, peak time, maximum overshoot/undershoot, and integral time square error in all scenarios. The STFTID controller decreased the ITSE index compared to the PID, TID, and I-TD in the first scenario down to 87.5%, 80%, and 68.2%, respectively, where a 1% step load is only applied to the first area of a two-area power system. For the second scenario, in which a multi-step load perturbation is forced onto area 1 of a two-area power system, ITSE decreased to 91.1% and 87.5% compared to the TID and I-TD controllers. In the third scenario, considering renewable power plants, this parameter was reduced to 55.3% and 46.5%, respectively. In this scenario, load disturbances were applied with various rectangular functions at different time intervals, and wind and PV power plants were connected at different times. For the last scenario, a communication time delay and two-step load disturbances were forced onto the controller's output, in addition to connecting the PV and wind power plants at other time steps. This scenario also exhibits the better performance of the STFTID system, with a 76.2% and 67.8% reduction in the ITSE compared to the TID and I-TD controllers, respectively. Overall, the proposed STFTID controller presents more sustainability than other control methods.

## REFERENCES


[1] Y. Arya, R. Ahmad, I. Nasiruddin, and M. F. Ahmer, "LFC performance advancement of two-area RES penetrated multi-source power system utilizing CES and a new CFOTID controller," Journal of Energy Storage, Vol. 87, p. 111366, 2024.

[2] R. Singh, J. Kumar, J. Singh, and G. S. Chaurasia, "Renewable Energy - Based Load Frequency Controller and Model with a Reduced Order for a Large - Scale Power System," Energy Technology, Vol. 12, No. 1, p. 2300618, 2024.

[3] M. Khamies, A. H. Elkasem, M. H. Hassan, and S. Kamel, "Enhancing frequency stability in diverse power systems with conventional and renewable energy sources based on an innovative LFC and controlled energy storage integration," Journal of Energy Storage, Vol. 73, p. 108960, 2023.

[4] S. Biswas, P. K. Roy, and K. Chatterjee, "FACTS-based 3DOF-PID controller for LFC of renewable power system under deregulation using GOA," IETE Journal of Research, Vol. 69, No. 3, p. 1486-1499, 2023.

[5] G. Wang, C. Wang, Q. Hao, and M. Shahidehpour, "Load Frequency Control Method for Cyber-Physical Power Systems with 100% Renewable Energy," IEEE Transactions on Power Systems, 2023.

[6] A. M. A. Soliman, M. Bahaa, and M. A. Mehanna, "PSO tuned interval type-2 fuzzy logic for load frequency control of two-area multi-source interconnected power system," Scientific Reports, Vol. 13, No. 1, p. 8724, 2023.

[7] M. Ranjan and R. Shankar, "A literature survey on load frequency control considering renewable energy integration in power system: Recent trends and future prospects," Journal of Energy Storage, Vol. 45, p. 103717, 2022.

[8] A. A. Abou El-Ela, R. A. El-Sehiemy, A. M. Shaheen, and A. E.-G. Diab, "Design of cascaded controller based on coyote optimizer for load frequency control in multi-area power systems with renewable sources," Control engineering practice, Vol. 121, p. 105058, 2022.

[9] P. Sharma and S. Neeli, "Computation of stability boundary locus of robust PID controller for time delayed LFC system," International Journal of Dynamics and Control, p. 1-11, 2023.

[10] J. Ansari, M. Homayounzade, and A. R. Abbasi, "Load frequency control in power systems by a robust backstepping sliding mode controller design," Energy Reports, Vol. 10, p. 1287-1298, 2023.

[11] F. Amiri and M. H. Moradi, "Improving the MPC performance of the model in order to improve the frequency stability of the two-area microgrid," International Journal of Industrial Electronics Control and Optimization, 2024.

[12] A. M. Taher et al., "Optimal model predictive control of energy storage devices for frequency stability of modern power systems," Journal of Energy Storage, Vol. 57, p. 106310, 2023.

[13] A. Karimi, Y. Jafarian, H. Bevrani, and R. Mirzaei, "Frequency response improvement in microgrids: a fuzzy–based virtual synchronous generator approach," International Journal of Industrial Electronics Control and Optimization, Vol. 3, No. 2, p. 147-158, 2020.

[14] J. Vinitha, G. Ramadas, and P. U. Rani, "PSO based fuzzy logic controller for load frequency control in EV charging station," Journal of Electrical Engineering & Technology, Vol. 19, No. 1, p. 193-208, 2024.

[15] A. Karimipouya, S. Karimi, and H. Abdi, "Microgrid frequency control using the virtual inertia and ANFIS-based Controller," International Journal of Industrial Electronics Control and Optimization, Vol. 2, No. 2, p. 145-154, 2019.

[16] R. K. Singh and V. Verma, "ANN-tuned PIDN controller for LFC with modified HVDC tie-line in deregulated environment," International Journal of Information Technology, Vol. 15, No. 8, p. 4193-4210, 2023.

[17] B. Dhanasekaran, J. Kaliannan, A. Baskaran, N. Dey, and J. M. R. Tavares, "Load frequency control assessment of a PSO-PID controller for a standalone multi-source power system," Technologies, Vol. 11, No. 1, p. 22, 2023.

[18] J. Biswas, P. Bera, and K. Chakrabarty, "Determination of control area and design of fuzzy rule-tuned PID controller for LFC of multimachine power system," Electric Power Systems Research, Vol. 221, p. 109411, 2023.

[19] S. Korram and H. R. ezadfar, "Use of genetic algorithm in optimal control of real power and load angle of synchronous generator," International conference on recent trends in engineering and materials science, 2016, Dubai, UAE, p. 1-15.

[20] S. M. Hosseini, R. Abdollahi, and M. Karrari, "Inclusive design and implementation of online load angle measurement for real-time transient stability improvement of a synchronous generator in a smart grid,"

IEEE Transactions on Industrial Electronics, Vol. 65, No. 11, p. 8966-8972, 2018.
[21] M. Abdolhosseini and R. Abdollahi, "Design of HHO-PID Controllers for Load Angle of Power Plant Synchronous Generators," International Transactions on Electrical Energy Systems, Vol. 2022, No. 1, p. 7746062, 2022.
[22] R. Abdollahi, "Modeling by order reducing the load angle of a three-phase synchronous generator and designing an AOA-PID controller to control the load angle," Journal of Modeling in Engineering, Vol. 21, p 83-99, 2023.
[23] R. Choudhary, J. Rai, and Y. Arya, "Cascade FOPI-FOPTID controller with energy storage devices for AGC performance advancement of electric power systems," Sustainable Energy Technologies and Assessments, Vol. 53, p. 102671, 2022.
[24] A. Kumar and S. Pan, "Design of fractional order PID controller for load frequency control system with communication delay," ISA transactions, Vol. 129, p. 138-149, 2022.
[25] P. N. Topno and S. Chanana, "Load frequency control of a two-area multi-source power system using a tilt integral derivative controller," Journal of Vibration and Control, Vol. 24, No. 1, p. 110-125, 2018.
[26] A. Rai and D. K. Das, "The development of a fuzzy tilt integral derivative controller based on the sailfish optimizer to solve load frequency control in a microgrid, incorporating energy storage systems," Journal of Energy Storage, Vol. 48, p. 103887, 2022.
[27] S. A. Kumar, M. S. S. Narayana, and K. J. Gowd, "Application of a TID Controller for the LFC of a Multi Area System using HGS Algorithm," Engineering, Technology & Applied Science Research, Vol. 13, No. 3, p. 10691-10697, 2023.
[28] S. Semwal, A. Mittal, S. Kumar, S. Goyal, and A. Singh, "Comparative Analysis of Two-Area Load Frequency Control Using Tilted-Integral-Derivative (TID) and Proportional-Integral-Derivative (PID) Controllers," in 2024 1st International Conference on Trends in Engineering Systems and Technologies (ICTEST), 2024: IEEE, pp. 1-5.
[29] S. Kumari and G. Shankar, "Design of SSA Tuned Cascaded TI-TID Controller for Load Frequency Control of Multi-Source Power System with Electric Vehicle," Industrial Control Systems, p. 255-283, 2024.
[30] S. A. Kumar, M. S. S. Narayana, and K. J. Gowd, "Application of a TID Controller for the LFC of a Multi Area System using HGS Algorithm," Engineering, Technology & Applied Science Research, Vol. 13, No. 3, p 10691-10697, 2023.
[31] N. C. Patel and M. K. Debnath, "Whale optimization algorithm tuned fuzzy integrated PI controller for LFC problem in thermal-hydro-wind interconnected system," in Applications of Computing, Automation and Wireless Systems in Electrical Engineering: Proceedings of MARC 2018, 2019: Springer, p. 67-77.
[32] A. Rai and D. K. Das, "Ennoble class topper optimization algorithm based fuzzy PI-PD controller for micro-grid," Applied Intelligence, Vol. 52, No. 6, p. 6623-6645, 2022.
[33] K. Ullah, A. Basit, Z. Ullah, S. Aslam, and H. Herodotou, "Automatic generation control strategies in conventional and modern power systems: A comprehensive overview," Energies, Vol. 14, No. 9, p. 2376, 2021.
[34] N. Jalali, H. Razmi, and H. Doagou-Mojarrad, "Optimized fuzzy self-tuning PID controller design based on Tribe-DE optimization algorithm and rule weight adjustment method for load frequency control of interconnected multi-area power systems," Applied Soft Computing, Vol. 93, p. 106424, 2020.
[35] M. Ahmed, G. Magdy, M. Khamies, and S. Kamel, "Modified TID controller for load frequency control of a two-area interconnected diverse-unit power system," International Journal of Electrical Power & Energy Systems, Vol. 135, p. 107528, 2022.
[36] J. Morsali, K. Zare, and M. T. Hagh, "Performance comparison of TCSC with TCPS and SSSC controllers in AGC of realistic interconnected multi-source power system," Ain shams engineering journal, Vol. 7, No. 1, p. 143-158, 2016.
[37] J. Morsali, K. Zare, and M. T. Hagh, "Comparative performance evaluation of fractional order controllers in LFC of two-area diverse-unit power system with considering GDB and GRC effects," Journal of electrical systems and Information Technology, Vol. 5, No. 3, p. 708-722, 2018.
[38] S. Tavakoli, A.-A. Zamani, and A. Khajehoddin, "Efficient load frequency control in multi-source interconnected power systems using an innovative intelligent control framework," Energy Reports, Vol. 11, p. 2805-2817, 2024.

**Morteza Janfaza** received B.S., M.S., and Ph.D. degrees in Electrical Engineering from the University of Sistan and Baluchestan, Zahedan, Iran, in 2011, 2013, and 2019, respectively. He is currently an assistant professor in the Departement of Electrical Engineering, Higher Education Complex of Saravan, Saravan, Iran. His current research interests include graphene, nano-optics, plasmonics, optoelectronic devices, nanoelectronics, and sensors.

**Abbas-Ali Zamani** was was born in 1986 in Isfahan, Iran. He earned a B.Sc. degree in electronic engineering from Hakim Sabzevari University in Iran in 2009, and an M.Sc. degree in control engineering from Isfahan University of Technology in 2011. In 2018, he received his Ph.D. in control engineering from the University of Sistan and Baluchestan in Iran. Dr. Zamani is currently an assistant professor in the Department of Electrical Engineering, National University of Skills (NUS), Tehran, Iran. Seismic control, power system control, smart grids, renewable energies, and artificial intelligence are among his research interests.